

Finite element analysis of acoustic streaming through the driving force in an ultrasonic air pump.

WADA Yuji (1), KOYAMA Daisuke (1), NAKAMURA Kentaro (1)

(1) Precision and Intelligence Laboratory, Tokyo Institute of Technology
4259-R2-26 Nagatsutacho, Midori-ku, Yokohama, 226-8503 Japan, wada@sonic.pi.titech.ac.jp

PACS: 43.25.Nm

ABSTRACT

For the simulation of ultrasonic air pump, the effective amendment using finite element analysis (FEA) is suggested. The pump induces airflow in a thin gap between a bending transducer and a reflector by exciting an intense sound field. As to numerical calculation of the acoustic streaming, approximate model based on the driving force of the acoustic streaming has been used. However, in the case of flow within far thinner gap compared to the wavelength, this method no longer keeps the accuracy. In this paper, we suggest the amendment toward the conventional analysis method, where the effect of the term of the static pressure gradient is considered. The calculation shows that the flow of the air goes toward the sound pressure nodes, and then, as a result of the comparison with the measurement, it is in good agreement with the actual results in the shape of the flow distribution.

BACKGROUND

It has been known that medium fluid flows in accordance with the gradient of the sound field strength. This is called “acoustic streaming” and has been attracting theoretical and experimental interest.¹ At the same time, its effect plays an important role in some applications of high-power ultrasound.^{2,3,4,6,7} In recent years, devices, such as mobile terminals, have become smaller and thinner with more power consumption. This causes a demand for a low-profile air-supplying device, which supplies gas flows into a narrow space in which conventional fans or pumps cannot be embedded.⁵ We have suggested an ultrasonic air pump utilizing acoustic streaming.^{8,9,10} This device can be a solution to this problem since it requires only a vibrating plate and a reflector. A bending transducer is placed facing the reflector across a thin air layer, which excites an intense sound field and then produces acoustic streaming. To optimize the structure of the device, an appropriate simulation, which considers the viscous effect terms and expresses the absolute value of sound pressure is required.

We have reported numerical calculations based on the full-fluid dynamics, which predict absolute sound pressure distributions in the air layer and derive the acoustic streaming from the sound field directly by solving Navier-Stokes equations using finite element analysis (FEA).¹¹ However, this cost of the fluid dynamics calculations is so heavy that calculation time takes as long as 4.7 days even using the computer with quad-core processor. This makes almost impossible to obtain even simple characteristic of streaming, such as frequency response; to obtain stationarity which is stable enough from the restriction of simulation time, or to carry out analysis where the frequency of ultrasound is over 15 kHz from the restriction of calculation mesh density.

There is another way to calculate the acoustic streaming. It utilize a presumed force of acoustic streaming driving force calculated from sound field. Flow velocity is calculated by input it toward static flow analysis instead of the gravity. However, in the case of our ultrasonic air pump, this method doesn't work

well. We attributed this error to the neglect of static pressure distribution which appears in the thin air layer.

In this paper, we suggested the amendment for the calculation of the acoustic streaming of our ultrasonic air pump through the driving force to reduce the calculation cost and improve the accuracy of the calculation of conventional analysis method using FEA. Then, we made a validation of this method by comparing to the measurement result.

ACOUSTIC STREAMINGS AND DRIVING FORCE

When we excite the intense sound field, because of nonlinearity, sound field produces static pressure and static flow field. The former is called radiation pressure and the latter is acoustic streaming. The pressure distributions are expressed by sound pressure p_a , static pressure P_0 , and induced static component p_0 as follows:

$$p = p_a + P_0, \quad (1)$$

$$\bar{p} = P_0 = P_{atm} + p_0 \quad (p_0 \ll P_{atm}), \quad (2)$$

$$\bar{p}_a = 0, \quad (3)$$

where the P_{atm} is the pressure of the atmosphere, which is the static pressure infinitely away from the device.

The flow velocity distributions are expressed by sound particle velocity u_a , acoustic streaming velocity U , and vibrating component of density ρ_a as follows:

$$u = u_a + U - \frac{1}{\rho} \overline{\rho_a v_a}, \quad (4)$$

$$\bar{v}_a = \bar{\rho}_a = 0. \quad (5)$$

Substituting these equations into compressive Navier-Stokes equations, then taking the time average, finally neglect the third-order small parameters, we can handle the fluid whose velocity is U as incompressible, where the acoustic driving force F exists like the gravity as:

$$\text{div}U = 0 \quad (6)$$

$$\frac{\partial U}{\partial t} + (U \cdot \nabla)U - \frac{\eta}{\rho_0} \nabla^2 U = -\frac{\nabla P_0}{\rho_0} + F, \quad (7)$$

$$F = -\overline{(u_a \cdot \nabla)u_a} - \overline{u_a \text{div}u_a}. \quad (8)$$

This indicates that we can assume the behaviour of the air flow by the sound field, through the calculation of acoustic streaming driving force F and put it into incompressible fluid equations.

Generally, simulations of the acoustic streaming, $\frac{\nabla P_0}{\rho_0}$ can be regard as zero as long as there is no extra pressure gradient. However, as we will show in the result section, in the case we excite the high intensity sound in such a thin air layer, $\frac{\nabla P_0}{\rho_0} = \frac{\nabla p_0}{\rho_0}$ is so large compared to F that we no longer neglect this term. As a result, the conventional simulation method produces error such as flow run towards the antinodes of the sound field.

This time we consider the static pressure distribution, by addition of force from this static pressure $\frac{\nabla p_0}{\rho_0}$ to driving force as :

$$F_{eff} = -\overline{(u_a \cdot \nabla)u_a} - \overline{u_a \text{div}u_a} - \frac{\nabla p_0}{\rho_0} \quad (9)$$

CONFIGURATION OF THE DEVICE

The actual configuration of the device is illustrated in Fig. 1. The bending transducer consists of an aluminum plate and a piezoelectric zirconate titanate (PZT; Fuji Ceramics C-203) element bonded on the back of the aluminum plate. The aluminum plate is 30 mm in width, 20 mm in length, and 2 mm in thickness, and the PZT element is 30 mm in width, 10 mm in length, and 0.4 mm in thickness. We set the x -axis along the length direction, the y -axis along the width direction, and the z -axis normal to the plate; moreover, and we set the origin at the center of the plate in the middle of the air gap, as shown in Fig. 1. By driving the PZT element at the resonant frequency of 26.2 kHz, the fundamental bending vibration along the length direction is excited on the transducer. Figure 2 shows the vibration mode shape, where the vibration displacement is exaggerated.

The transducer is supported at the vibration nodes ($x = -6.0, +5.2$ mm, $y = \pm 15$ mm).

To maintain measurement conditions, the vibration velocity amplitude at the edge of the transducer ($x = +10$ mm, $y = -15$ mm) is measured using a laser Doppler vibrometer and adjusted to 0.5 m/s throughout the experiments (12.4 μm in peak-to-peak vibration displacement amplitude).

An acrylic resin plate with the same dimensions as the aluminum plate is firstly located parallel to the transducer with a gap of 1 mm and acts as a reflector. Then, as shown in Fig. 3, the reflector is tilted along the length direction within a range from 0 to 10 degrees to obtain the directional flow. In this paper, we concentrate on the case where the degree of the reflector tilt is 0 and 4 degrees.

When we excite the vibration on the transducer, the intense sound field is excited in the gap. The $(n_x, n_y) = (3, 1)$ mode sound pressure distribution was chosen to be excited in the gap, in which the $3\lambda/2$ and $\lambda/2$ resonance are generated in the length and width directions as shown in Fig. 4⁹ since the larger sound pressure is desired to obtain the large air flow, and large correlation between the vibration mode of the transducer and the sound pressure distribution induces the large sound pressure.

Because of this high amplitude sound, the degree of nonlinearity gets larger and then the constant component of flow appears, as if there exist the force field F in eq. (8) and drives the air particle into the streaming.

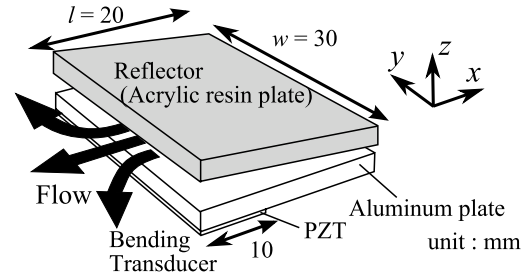


Figure 1: Basic structure of the device.

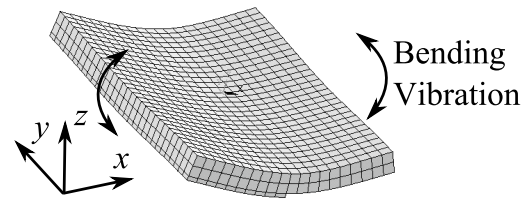


Figure 2: Bending vibration mode on the transducer.

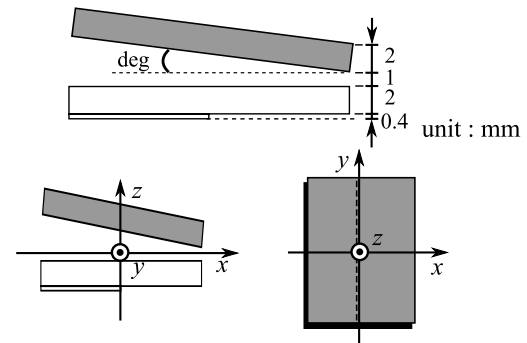


Figure 3: Configurations of reflectors.

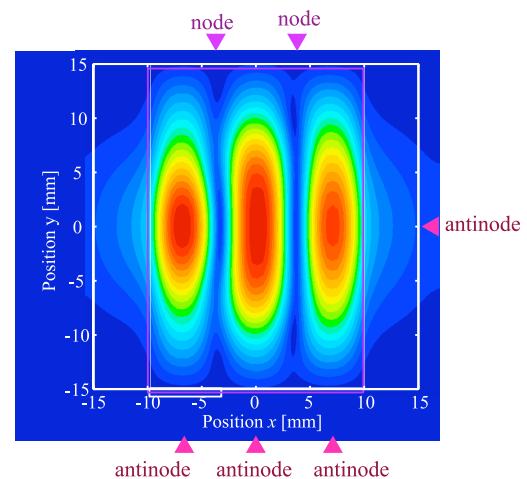


Figure 4: (3, 1) mode sound pressure distribution in the air gap.

ANALYSIS METHOD

Outline

Figure 5 shows the block diagram of the analysis, and the outline is as follows.

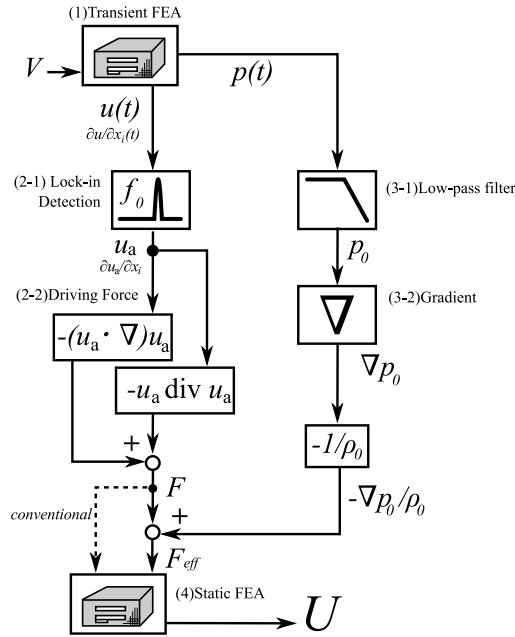


Figure 5: The block diagram of the analysis

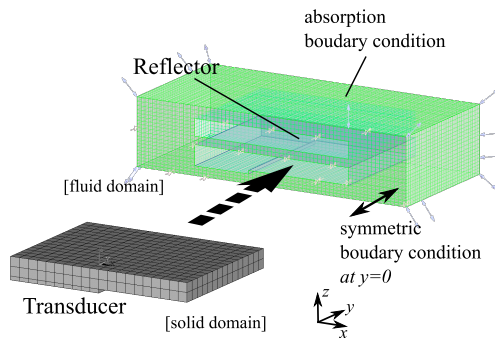


Figure 6: Transient FEA model.

- 1 By finite element transient analysis, calculate the temporal waveform of the pressure distribution $p(t, x, y)$ and velocity distribution $u(t, x, y)$.
- 2-1 By simulated lock-in detection to the temporal waveform of the velocity distribution, obtain the complex particle velocity distribution $u_a(x, y)$.
- 2-2 From the eq. (8), calculate the driving force without revision F .
- 3-1 By low-pass filtering to the temporal waveform of the pressure distribution, obtain the static pressure distribution $p_0(x, y)$.
- 3-2 By taking numerical differential of the static pressure distribution and divide them by the static density of air ρ_0 , obtain the force from the static pressure $-\nabla p_0(x, y)/\rho_0$.
- 4 By adding two force F and $-\nabla p_0(x, y)/\rho_0$, obtain the revised driving force in eq. (9). Finally, by inputting into static flow analysis by finite element analysis, obtain the acoustic streaming distribution $U(x, y)$.

The most important amendment we suggest in this paper is the effect of $-\nabla p_0(x, y)/\rho_0$ in step 4; therefore, we compare the calculation where the amended driving force F_{eff} inputted in step 4, and the one where the conventional driving force F inputted in step 4.

1. Transient analysis of fluid by FEA

The motion of the air and transducer is simulated by a piezoelectric-structure-fluid interaction analysis model using the commercial FEA software ANSYS 11.0 MFX-ANSYS/CFX (ANSYS, Inc.). Then, the temporal waveforms of the pressure and velocity of the air are achieved by this analysis. The FEA simulation consists of two main analysis routines, which are linked together. The first routine simulates the vibration of the transducer by the piezoelectric-structure interaction analysis model side and passes the result for the displacement to the second routine. Then, the second routine simulates the motion of the air under the fluid dynamics and passes the result for the pressure to the first routine.

The configurations of transient FEA are as follows. The models of the transducer and reflector are surrounded by an air block ($35 \times 33 \times 8 \text{ mm}^3$), as shown in Fig. 6. Even though size is rather smaller than is required to simulate acoustic streaming itself, it was found to be large enough to maintain the calculation accuracy of the sound pressure, particle velocity and static pressure. This reduces the calculation time cost from 4.7 days to 1.3 days. The transducer, reflector, and the air block are divided in a 0.5 mm mesh. The calculation time step (Δt) for the transient analysis is $1 \mu\text{s}$ (38.1 times per driving ultrasound cycle). The total simulation time is 4 ms (104.8 cycles).

With respect to the boundary, the following conditions are applied. The absorbing boundary condition is adopted at the outer surface of the surrounding air block to express the infinite region.^{19,20} The symmetric boundary condition at the $y=0$ plane is adopted and spares half of the model to reduce the amount of calculation. The perfect reflection is assumed for the reflector. The no-slip condition at the boundary between air and other materials considering the viscous effect is applied.

2-1. Particle velocity through simulated lock-in detection

The sound pressure in the complex number is obtained from the temporal waveform of the pressure $p(t)$ by the simulated lock-in detection

$$u_a = \frac{1}{2} \overline{u(t) \cos(\omega t)} - j \frac{1}{2} \overline{u(t) \sin(\omega t)}, \quad (10)$$

where $j^2 = -1$, and ω is the driving angular frequency. The operation of time average is substituted by the application of a low-pass filter, and the final value is used as the result for the sound pressure. The low-pass filter is the fifth Butterworth low-pass filter. The cutoff frequency is 6.45 kHz, which is 1/2 of the driving frequency.

2-2. Driving force

The space differentials of velocity such as ∇u which is needed to calculate the driving force in eq. (8), can be obtained as a result of transient FEA. Therefore, by substituting the expression as follows:

$$\{(u_a \cdot \nabla) u_a\}_i = u_a \frac{\partial u_i}{\partial x} + v_a \frac{\partial u_i}{\partial y} + w_a \frac{\partial u_i}{\partial z} \quad i \in (x, y, z), \quad (11)$$

$$\text{div} u_a = \frac{\partial u_x}{\partial x} + \frac{\partial u_y}{\partial y} + \frac{\partial u_z}{\partial z}, \quad (12)$$

and operating time average using the same low-pass filter as one used in simulated lock-in detection, the driving force is calculated.

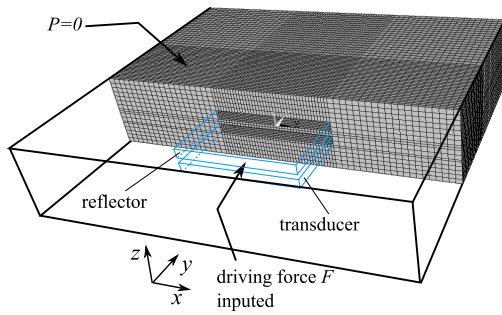


Figure 7: Static FEA model.

3-1. Static pressure through low-pass filter

The static pressure distribution is obtained from eq. (2). For the calculation of time average, the fifth Butterworth low-pass filter whose cutoff frequency is 1.29 kHz, which is 1/10 of the driving frequency, is used.

3-2. Static pressure gradient

To calculate the differential of static pressure gradient numerically, we differentiate them using discrete Fourier transform and invert discrete Fourier transform, instead of finite difference method to keep the signal-to-noise ratio in the analysis result.

$$\frac{\partial P_0}{\partial x_i} = \text{Re} \left\{ \mathcal{F}_i^{-1} [j k_i w(k_i) \mathcal{F}_i \{P_0\}] \right\}, \quad (13)$$

where $i \in (x, y, z)$ is the coordinate symbol, $k_0 = 2\pi/\lambda$ is the angular wave number of ultrasound in the air, Fourier and Invert Fourier transform to the function of position $f(x)$ and $G(k)$ in the wave number space is as follows, respectively:

$$\mathcal{F}_i \{f(x_i)\} = F(k_i) = \int_{-\infty}^{\infty} f(x_i) e^{-jk_i x_i} dx_i, \quad (14)$$

$$\mathcal{F}_i^{-1} \{G(k_i)\} = g(x_i) = \frac{1}{2\pi} \int_{-\infty}^{\infty} G(k_i) e^{jk_i x_i} dk_i, \quad (15)$$

and the rectangular window function $w(k_i)$ which works as a low-pass filter is:

$$w(k_i) = \begin{cases} 1 & -1.5k_0 \leq k_i \leq 1.5k_0 \\ 0 & \text{otherwise.} \end{cases} \quad (16)$$

4. Acoustic streaming

To simulate the motion of air under the eq. (7), finite element static flow analysis is carried out using the commercial FEA software ANSYS 11.0 (ANSYS Inc.). Then, we achieve the acoustic streaming velocity U as result of this analysis.

The configurations of static FEA are as follows. The models of the transducer and reflector are surrounded by an air block ($70 \times 60 \times 15 \text{ mm}^3$), as shown in Fig. 7. With respect to the boundary, the following conditions are applied. The transducer, reflector, and the air block are divided in a 0.5 mm mesh.

The static pressure is set to zero at the outer surface of the surrounding air block to express open region. The perfect reflection is assumed for the reflector. The no-slip condition at the boundary between air and other materials considering the viscous effect is applied. As for driving conditions, the driving force F or F_{eff} is set as a nodal body force load.

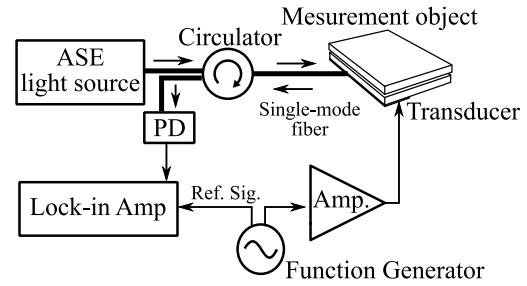


Figure 8: Measurement setup for sound pressure.

EXPERIMENTAL METHODS

Sound pressure

The sound pressure distribution in the gap is measured using an optical fiber probe with a diameter of $125 \mu\text{m}$.²¹ The measurement system used is shown in Fig. 8. Since the change in pressure causes refractive-index modulation, sound pressure in absolute figures is measured by the reflectance modulation of the fiber optics. The sound pressure is measured every 1 mm for the regions $-15 \text{ mm} < x < 15 \text{ mm}$ and $-15 \text{ mm} < y < 15 \text{ mm}$.

Flow velocity

The shape of the flow distribution in the gap was measured by particle image velocimetry (PIV). Lycopodium spore powder was set on the transducer as tracers. Then, the induced acoustic streaming of air carried the powder. The motion of powder was captured with a high-speed camera under light-emitting diode illumination. To reduce the effect of vibration itself, the capture rate of the image was set to 1310 frame per second, which is 1/20 of the driving frequency. The exposure time was set to $10 \mu\text{s}$ and 1500 frames (1.15 s) were captured. The areas of $-20.1 \text{ mm} < x < 21.3 \text{ mm}$, $-15.9 \text{ mm} < y < 14.7 \text{ mm}$ were captured into a 512×384 pixel image.

The PIV calculations were carried out as follows. The images were divided in a 5×5 pixel ($0.414 \times 0.414 \text{ mm}^2$) grid and the pattern of that region was traced. From the traced pattern displacement and the capture rate, we obtained the flow velocity fields. Finally, to reduce the amount of noise, the velocity fields were averaged through all the frames and incorrect vectors are removed.

ANALYSIS AND EXPERIMENTAL RESULT

Sound pressure

Figure 9 and 10 shows the calculation result of the sound pressure distribution in the air gap. (3, 1) resonance mode sound pressure distributions are observed, where we find the antinode at $x=0 \text{ mm}$, $\pm 7 \text{ mm}$, and nodes at $x = \pm 3.5 \text{ mm}$. Figure 11 show the calculation and measurement result on x -axis. The calculation agree well with measurement. While the sound pressure distribution is standing wave when 0 degree, traveling wave component toward the left is observed when 4 degrees.

Driving force

Figure 13 and 14 shows the calculation result of the acoustic streaming when the gradient of the reflector is 0 degree and 4 degrees respectively. The color of vectors mean the degree of x -component of driving force, that is, red vectors indicates right-hand force, blue vectors indicates left-hand force, and white vectors indicates the force normal to the x -axis. From both re-

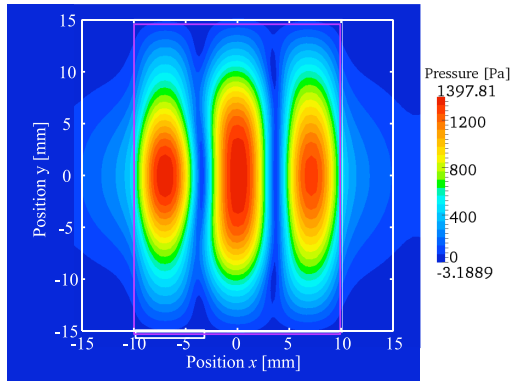


Figure 9: Calculation result of sound pressure distribution when the gradient of the reflector is 0 degree.

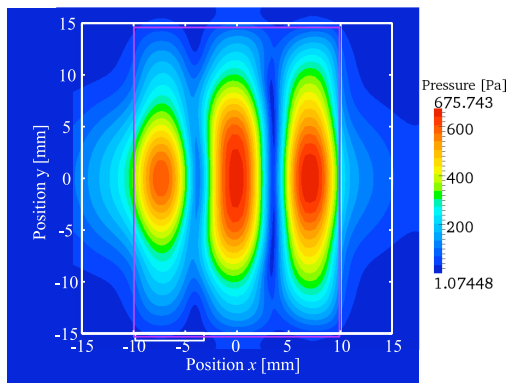


Figure 10: Calculation result of sound pressure distribution when the gradient of the reflector is 4 degree.

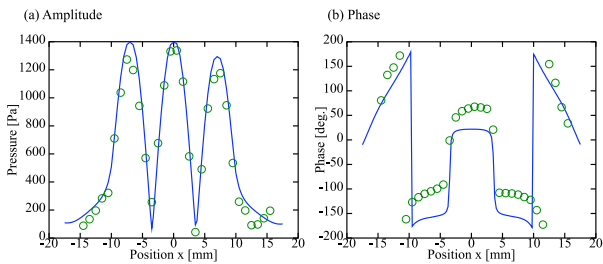


Figure 11: Calculation and measurement result of sound pressure (a) amplitude and (b) phase distribution on x-axis when the gradient of reflector is 0 degree.

result vectors toward antinode of the sound pressure distribution shown in Fig. 9 and 10 was observed. From the distribution when the gradient of the reflector is 0 degree, almost symmetric distribution is observed; while the distribution when the gradient of the reflector is 4 degree, the vectors around left-side antinode is smaller than ones around other antinode.

Static pressure and its gradient

Figure 15, 16 shows the static pressure distribution p_0 indicated by the contour distribution and its gradient $-\nabla p_0$ indicated by black vectors when the gradient of the reflector is 0 degree and 4 degrees. From both result static pressure distri-

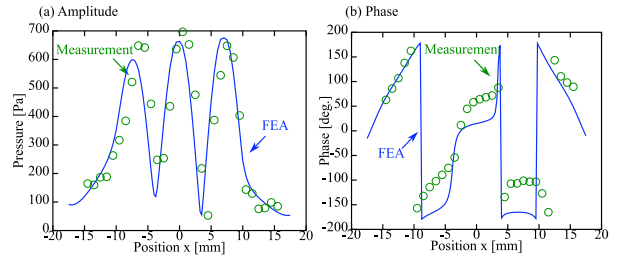


Figure 12: Calculation and measurement result of sound pressure (a) amplitude and (b) phase distribution on x-axis when the gradient of reflector is 4 degree.

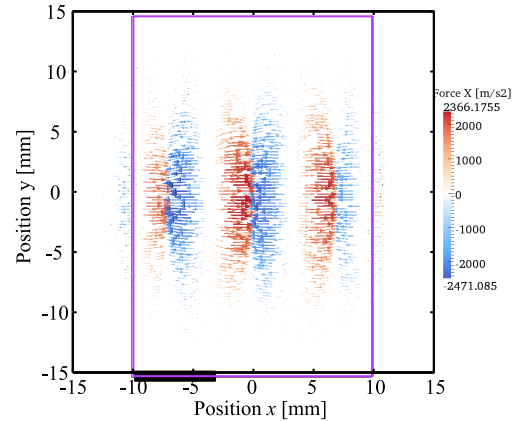


Figure 13: Calculated driving force F distribution when the gradient of the reflector is 0 degree.

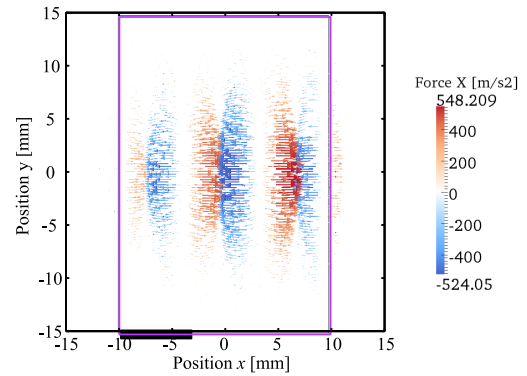


Figure 14: Calculated driving force F distribution when the gradient of the reflector is 4 degree.

butions has mainly three maxima and two minima is observed on the x-axis, and their gradients points from antinode towards node of the sound pressure distribution shown in Fig. 9 and 10. From the distribution when the gradient of the reflector is 0 degree, almost symmetric distribution is observed; while the distribution when the gradient of the reflector is 4 degree, the left-side maxima is smaller and the right-side maxima is larger than the maxima at the center.

Total driving force

Figure 17, 18 shows the amended driving force F_{eff} when the gradient of the reflector is 0 degree and 4 degrees. The color of vectors mean the degree of x-component of driving force as we showed in Fig.13 or 14. Figure 19, 20 shows x-component

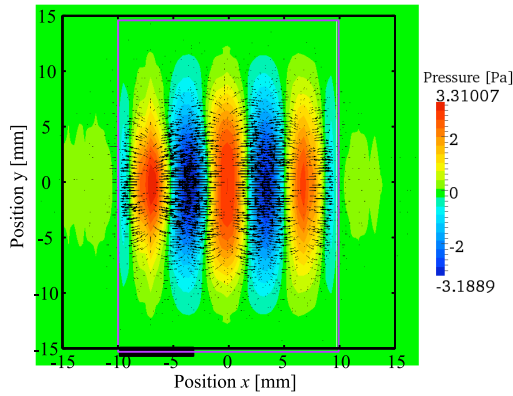


Figure 15: Calculated static pressure and its gradient distribution when the gradient of the reflector is 0 degree.

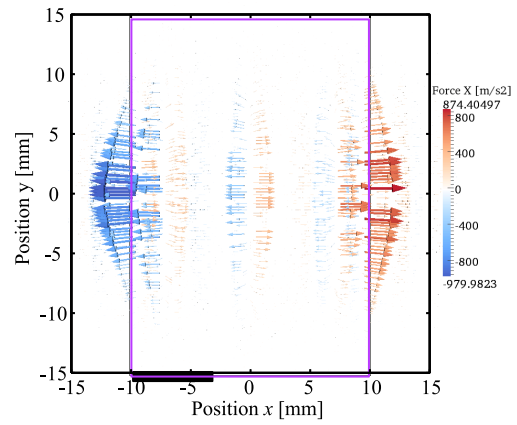


Figure 17: Calculated amended driving force F_{eff} distribution when the gradient of the reflector is 0 degree.

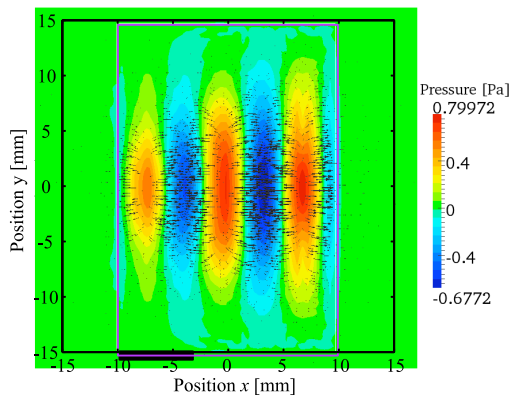


Figure 16: Calculated static pressure and its gradient distribution when the gradient of the reflector is 4 degree.

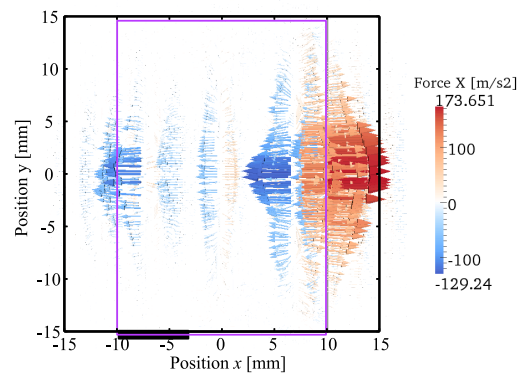


Figure 18: Calculated amended driving force F_{eff} distribution when the gradient of the reflector is 4 degree.

of the driving force F and the amendment $-\nabla p_0/\rho_0$, and the amended driving force F_{eff} when the gradient of the reflector is 0 degree and 4 degrees. As a result of addition of driving force F and static pressure gradient $-\nabla p_0/\rho_0$ main vectors which point towards/from antinode canceled out, then vectors which drives fluid directly remained. These vector mainly pointed towards outside of the device or towards nodes of the sound pressure distribution shown in Fig. 9 and 10. From the distribution when the gradient of the reflector is 0 degree, almost symmetric distribution is observed; while the distribution when the gradient of the reflector is 4 degree, blue vectors, which indicate force toward left, are spread in almost all part of airgap though there exist some large red vectors at the right edge of the device.

Result of flow analysis

Flow at the 0 degree

Figure 21 shows the measurement result of acoustic streaming distribution by PIV, Fig. 22 shows the result of static flow distribution calculated in conventional way, and Fig. 22 shows the result of static flow distribution calculated in the way suggested in this paper, when the gradient of reflector is 0 degree. White cloud appears in the Fig. 21 is powder used as a tracer of PIV and flow velocity vectors measured by are plotted in the figure.

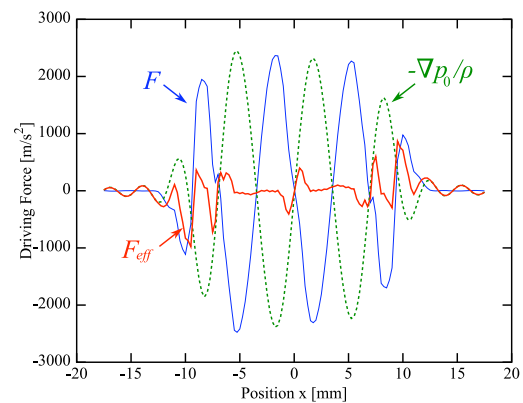


Figure 19: Calculated driving force X distributions on x-axis when the gradient of the reflector is 4 degree.

From the conventional result, Fig.22, vectors are observed which emitted from nodes of sound field and absorbed to antinodes of sound field. This means flow is compressible, which is against what is proposed in eq.(6). On the other hand, from the suggested result, Fig.22, such compressible behavior is dissolved, and some vectors toward the nodes are observed, which is also observed in the measurement as powder remains at the node.

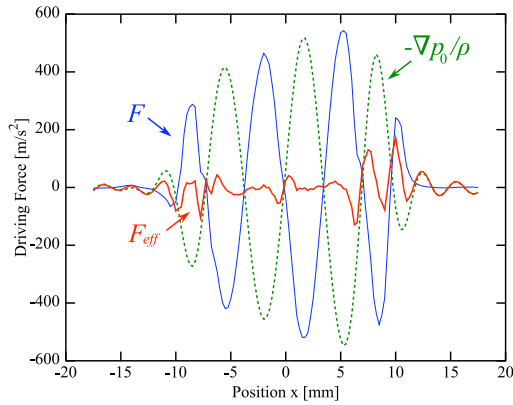


Figure 20: Calculated driving force X distributions on x-axis when the gradient of the reflector is 4 degree.

Flow at the 4 degrees

Figure 24 shows the measurement result of acoustic streaming distribution by PIV, Fig. 25 shows the result of static flow distribution calculated in conventional way, and Fig. 25 shows the result of static flow distribution calculated in the way suggested in this paper, when the gradient of reflector is 0 degree.

From the conventional result, Fig.25, vectors are observed which emitted from nodes of sound field and absorbed to antinodes of sound field, again here. On the other hand, from the suggested result, Fig.22, such compressible behavior is dissolved. Most vectors flow from front (-y) and back (+y) edge of the device at right node of the sound field, and then flow through the center of the node of the sound field, then flow toward right and left edge of the transducer. This is also observed in measurement Fig.24, so the suggested result is in good agreement with measurement.

CONCLUSION

In this paper, we suggested the amendment for the calculation of the acoustic streaming of our ultrasonic air pump through the driving force to reduce the calculation cost and improve the accuracy of the calculation of conventional analysis method using FEA. We made a validation by calculating the acoustic streaming induced by the ultrasonic air pump by both way, the conventional and the suggested way, and compared with the measurement. As a result, we reduced the calculation time by one-fourth, and the way we suggested successfully simulated the acoustic streaming to the point, such as flow around the node and antinode of the sound field, or degree of concentration of the flow, which the conventional way cannot calculated accurately.

REFERENCES

[1] W. L. Nyborg: J. Acoust. Soc. Am. **25** (1953) 68.
 [2] T. Hasegawa, J. Friend, K. Nakamura, and S. Ueha: Jpn. J. Appl. Phys. **44** (2005) 4658.
 [3] Y. Imamura, S. Sakamoto, and Y. Watanabe: Jpn. J. Appl. Phys. **46** (2007) 4417.
 [4] R. Ozaki, T. Shinpo, M. Ozaki, and H. Moritake: Jpn. J. Appl. Phys. **47** (2008) 1363.
 [5] R. Luharuka, C.-F. Wu, and P. J. Hesketh: Sens. Actuators **112** (2004) 187.
 [6] D. Köster: SIAM J. Sci. Comput. **29** (2007) 2352.

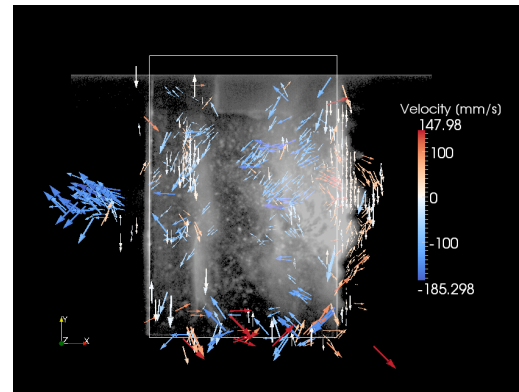


Figure 21: Flow distribution measured by PIV when the gradient of the reflector is 0 degree.

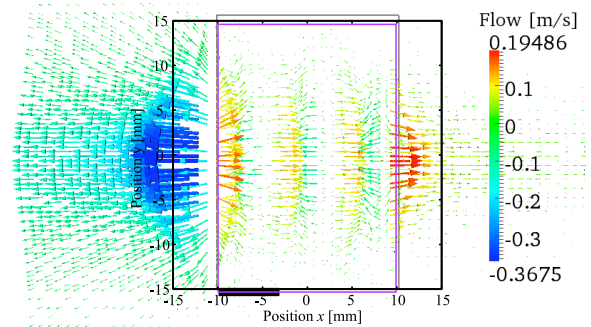


Figure 22: Flow distribution calculated in conventional way when the gradient of the reflector is 0 degree.

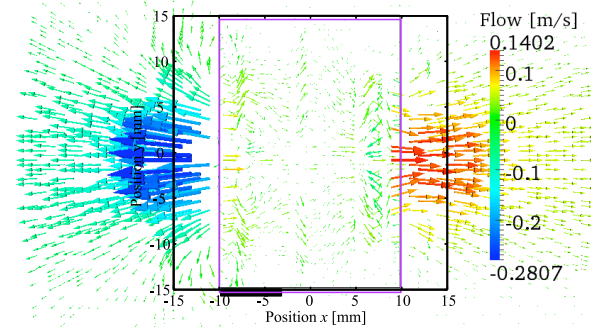


Figure 23: Flow distribution calculated in suggested way when the gradient of the reflector is 0 degree.

[7] T. Frommelt, D. Gogel, M. Kostur, P. Talkner, P. Hänggi, and A. Wixforth: IEEE Trans. Ultrason. Ferroelectr. Freq. Control. **55** (2008) 2298.
 [8] H. Takei, D. Koyama, K. Nakamura, and S. Ueha: Jpn. J. Appl. Phys. **47** (2008) 4276.
 [9] H. Takei, D. Koyama, K. Nakamura, and S. Ueha: *Denshi Joho Tsushin Gakkai Ronbunshi A* **91** (2008) 1152 [in Japanese].

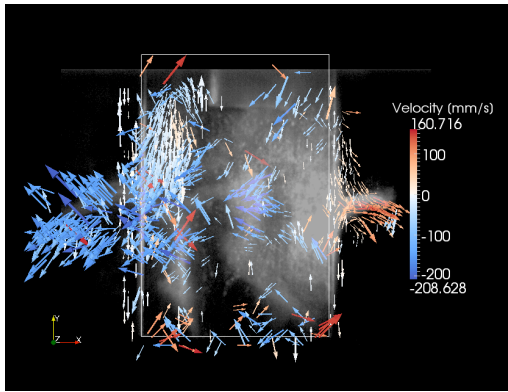


Figure 24: Flow distribution measured by PIV when the gradient of the reflector is 4 degree.

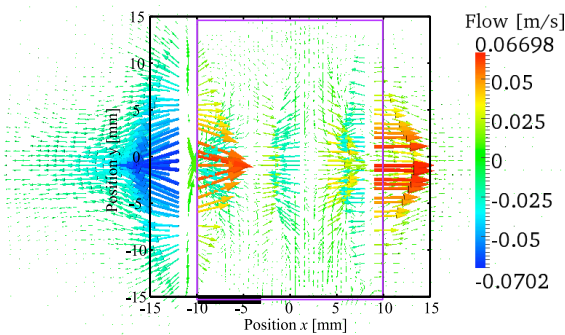


Figure 25: Flow distribution calculated in conventional way when the gradient of the reflector is 4 degree.

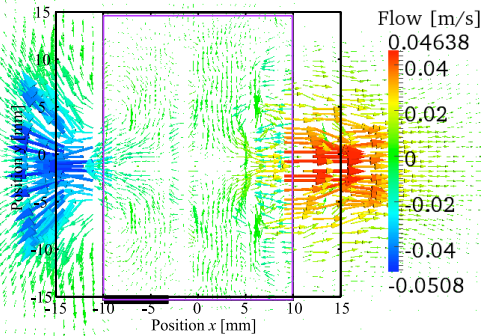


Figure 26: Flow distribution calculated in suggested way when the gradient of the reflector is 4 degree.

[10] D. Koyama, Y. Wada, K. Nakamura, M. Nishikawa, T. Nakagawa and H. Kihara: IEEE Trans. Ultrason. Ferroelectr. Freq. Control. **57** (2010) 253.

[11] Y. Wada, D. Koyama, K. Nakamura: to be published in Jpn. J. Appl. Phys..

[12] T. Hayasaka and S. Yoshikawa: *Onkyo Shindo-ron* (Theory of Acoustics and Vibrations) (Maruzen, Tokyo, 1974) p. 696 [in Japanese].

[13] J. Saito, J. R. Friend, K. Nakamura, and S. Ueha: Jpn. J. Appl. Phys. **44** (2005) 4666.

[14] T. Hasegawa, D. Koyama, K. Nakamura, and S. Ueha: Jpn. J. Appl. Phys. **46** (2008) 4931.

[15] T. Hasegawa, D. Koyama, K. Nakamura, and S. Ueha: Jpn. J. Appl. Phys. **47** (2008) 4248.

[16] T. Kozuka, K. Yasui, T. Tuziuti, A. Towata, and Y. Iida: Jpn. J. Appl. Phys. **46** (2008) 4948.

[17] D. Koyama, H. Takei, K. Nakamura, and S. Ueha: IEEE Trans. Ultrason. Ferroelectr. Freq. Control. **55** (2008) 1823.

[18] O. V. Rudenko and S. I. Soluyan: *Theoretical Foundations of Nonlinear Acoustics* (Plenum, New York, 1977).

[19] K. W. Thompson: Comput. Phys. **89** (1990) 439.

[20] T. J. Poinsot and S. K. Lele: Comput. Phys. **101** (1992) 104.

[21] H. Takei, T. Hasegawa, K. Nakamura, and S. Ueha: Jpn. J. Appl. Phys. **46** (2007) 4555.